ANALYSIS OF ENERGY DISSIPATION AND DEPOSITION IN ELASTIC BODIES IMPACTING AT HYPERVELOCITIES

David F. Medina and Firooz A. Allahdadi

Space Kinetic Impact and Debris Branch (PL/WSSD)
Phillips Laboratory, Kirtland AFB, NM 87117-6008

ABSTRACT

A series of impact problems were analyzed using the Eulerian hydrocode CTH. The objective was to quantify the amount of energy dissipated locally by a projectile-infinite plate impact. A series of six impact problems were formulated such that the mass and speed of each projectile were varied in order to allow for increasing speed with constant kinetic energy. The properties and dimensions of the plate were the same for each projectile impact. The resulting response of the plate was analyzed for global KE, global momentum and local maximum shear stress. The percentage of energy dissipated by the various HVI phenomena appears as a relative change of shear stress at a point away from the impact in the plate.

INTRODUCTION

A hypervelocity impact (HVI) between two bodies of large relative size is characterized by severe localized phenomena such as material phase change, jetting and high strain rate. Until the impacting bodies reach this relative velocity range (7 to 12 km/s), these phenomena will not be as pronounced. In this case, the energy deposited by the projectile will not have these avenues of dissipation. In this paper, we have divided the process of HVI into an early-time and a late-time phase. This division will facilitate the understanding of the kinematics leading from the early-time phase to the late-time phase where breakup of a satellite is most likely.

The early-time phase includes those effects which occur during the first 3 to 4 μs of a hypervelocity impact (projectile speed greater than 5 km/s). The kinematics of the early-time phase are restricted to the area of impact. Global response does not yet occur at this time especially for large relative size difference between the target and the impactor.

The late-time phase occurs when the stress waves induced by the impact have had a chance to propagate outward to a distance of about 16 diameters of the projectile. At this time, the phenomena occurring at the impact site have begun to stabilize. Also, at this distance and further from the area of impact, the deformations are not as severe and there is certainly no hydrodynamic behavior of the material.

The quantity and rate of energy deposition required to cause the breakup of an orbiting spacecraft is a function of the impactor's speed, mass and shape. An understanding of the deposition and dissipation of energy in a structure from an impact will allow us to understand and predict the post-impact propagation of energy-containing stress waves throughout the structure at latter times. Therefore, the scope of this study does not seek to explain the early-time phenomena, but rather the effect that these local phenomena have on the overall global response. The severity of the global response to a given amount of KE deposition will depend on the localized early-time dissipation of this KE. An example of a well-known localized dissipative effect absorbing much of the energy of an impact is the collapse of voids in a porous material [2]. Porous materials are used as shielding since voids in the material collapse and absorb much of the energy deposited by an impact. Therefore, less damage-producing energy is left to propagate throughout the structure.

PROBLEM FORMULATION

The 2 and 3-D hydrodynamic code CTH [1] was used to model a series of projectile impacts onto a plate. The speed and mass of the projectiles were varied but KE was held constant. The series of two-dimensional models which were set up had the initial conditions shown in Table 1. The projectiles for the six cases were represented with a circle which can be thought of as an infinite cylinder in three dimensions. The projectiles impacted in a direction normal to the plate surface. Since the models are two-dimensional, mass, kinetic energy and momentum are on a per unit length basis. The location on the mesh of the plate and projectile for case 1 is shown in Figure 1. The left boundary of the mesh ends at 5 cm although the plotting program extended

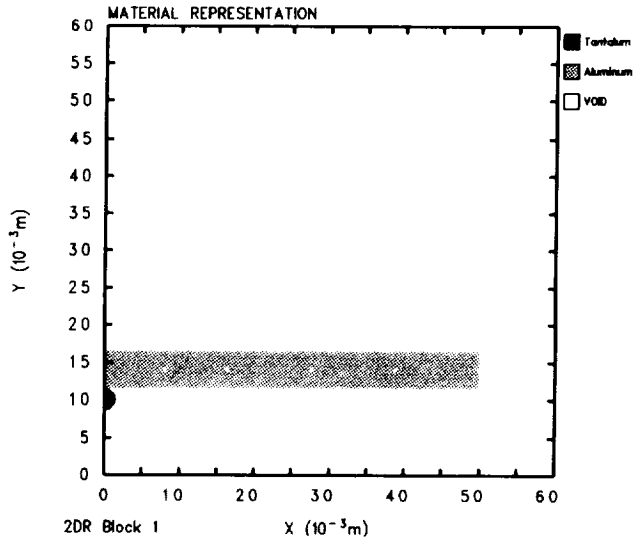

Figure 1. Model configuration of Case 1 at t=0.0

C-5

Projectile	Diameter (cm)	Speed (km/s)	Mass (g)	Kinetic Energy (kJ)	Momentum Kg-m/s (X-axis)
1	0.15	14.0	1.178	115.45	16.49
2	0.35	6.00	6.414	115.45	38.48
3	0.55	3.82	15.84	115.45	60.48
4	0.75	2.80	29.45	115.45	82.47
5	0.95	2.21	47.25	115.45	104.46
6	1.15	1.83	69.25	115.45	126.45

Table 1. Initial Conditions.

	Projectile	Target
Material:	Elemental tantalum	Elemental Aluminum
Shape:	Cylinder	Plate, 0.5 cm thick
Density:	16.6667 g/cm^3	2.713 g/cm^3
Equation of state:	Mie-Gruneisen	Mie-Gruneisen
Fracture model:	Max pressure criteria	Max pressure criteria
Strength model:	Elastic-plastic	Elastic-plastic

Table 2. Physical properties of the target and projectile models.

the plot frame to 6 cm. The points along the mid-section of the plate are Lagrangian tracer points at which stress was monitored. A plane of symmetry or 'mirror image' was defined along the left side of the mesh while the right side of the mesh was defined as a nonreflective boundary. These boundary definitions allow the modeling of an infinite plate. The mesh cell size was 0.5 mm x 0.5 mm (2-D cartesian). The physical properties of the plate and projectile are listed in Table 2. Tantalum was chosen as the material for the projectile because of its high yield and fracture strengths. For the scope of this study, it was best that the projectile remain as intact as possible since we were only interested in the response of the plate.

NUMERICAL RESULTS

The projectile in Case 1 had the highest speed and was the only one to induce localized phase changes. Figure 2 shows the progress of the impact for Case 1 at 1.27 μs. The darkly shaded region represents the material of the projectile and the plate material is shown in a lighter shade. It appears in Figure 2 that part of the aluminum plate has migrated onto the path of the projectile after it has passed through. This is explained by referring to Figure 3 which is a density representation of the same projectile-plate model at the same time (1.27 μs) as in Figure 2. The spacing of the dots in Figure 3 is proportional to the density of the material as shown by the legend on the upper right corner of the plot. From Figure 3 it can be seen that the material behind the projectile, directly in its path, is of much lower density than the solid aluminum making up the rest of the plate. This indicates that a phase change of the aluminum is occurring here due to the tremendous amount of kinetic energy deposited at this local.

The occurrence of phase change is further substantiated by Figure 4. The projectile-plate model is overlaid with maximum shear stress contours. Each contour represents a region of constant shear stresses which are quantified in the legend on the right. The darkest region represents the materials of the plate and projectile. The lightest contour represents the lowest value of stress among the eight contour values. It is seen from Figure 4 that the stress concentration on the aluminum plate is decreasing in the direction towards the impact site. After the lightest contour, there is no representable stress further on. This substantiates the fact that the material in this region has undergone a phase change and is no longer able to support shear stress waves since it is no longer solid. It will be shown below that a slower projectile impact at this same time will support shear stress waves closer in to the projectile-plate contact interface. Finally, phase change is also apparent by studying the particle velocity vectors at 1.27 μs in Figure 5. The random directions of the vectors behind the projectile along its path suggest the behavior of a non-solid material phase.

The decreased speed of the projectile in Case 2 did not induce localized phase changes. In this case, the aluminum material of the plate near the impact site did not migrate onto the path of the projectile (see Figure 6). The density representation at 1.26 μs is shown in Figure 7. The time of this plot (1.26 μs) corresponds closely to the time of the density plot of the preceding case (Figure 3). To be noted in Figure 7 is the uniformity of the density of the materials in the region of the impact. This indicates a lack of phase change occurring in the materials at this time. Also, unlike the previous case, shear stress waves can now propagate closer to the projectile-plate contact interface since the materials are still in a solid state (compare Figure 4 with Figure 8).

Kinetic energy versus time was calculated and plotted for the plate and projectile in each of the six cases (see Figures 9 and 10). The dropping off of each curve in these figures after a level section of constant KE is not a physical phenomena. This is caused by pieces of mass leaving the active mesh zone and therefore no longer accounted for in the energy calculations. A comparison of the curves of the KE of the projectiles with their respective plates indicates that energy is indeed being conserved. Figures 9 and 10 indicate that the faster and lighter projectiles are more effective at transferring their KE into the plate. However, we cannot conclude from these figures that the quantity of the late-time propagated energy will be greater for the smaller lighter projectiles. The KE calculation on the plate as a function of time is insensitive to concentrations of KE in the plate since the calculation is a summation over the entire plate material including unattached fragments within the mesh. Kinetic energy producing phase changes may be concentrated at the impact site and dissipated locally and may not propagate extensively. Since the initial KE of the projectiles is constant, the

difference in the amount of KE in the plate after impact should be due only to the behavior of the material in the projectile. Also, the projectile will carry away some KE after perforation. Perforation occurred for all six projectile impacts but at different times as indicated by the stabilization times of the KE curves in Figure 9. The amount of KE in the plate was conserved at a constant level after each projectile had perforated the plate.

The lighter and faster projectiles were also more effective at transferring momentum to the plate as shown in Figure 11. Figure 11 is a plot of the momentum of the center-of-mass of the projectile in the direction of its path versus time. Since KE is proportional to the square of the velocity and momentum is proportional to velocity, it was not possible to maintain a constant initial momentum for the projectiles while keeping KE constant (see Table 1). However, KE energy rather than momentum will affect the local region of impact to a greater extent than momentum. Wu and Simons make a statement in [2] which describe this phenomena, ". . . a projectile or particle beam will deliver both momentum and energy to a target. The target will absorb the momentum through an increase in its mass mean velocity, dV_i, but dV_i is generally so small that the associated kinetic energy $(dV_i)^2$ is much less than the energy of the impact. The target must dissipate the impact energy at the site of the impact load. This dissipation mechanism is generally the strain energy of the target volume." For this reason, KE was held constant since it plays the greatest role in affecting the local region of impact.

Phenomena occurring at the site of impact which dissipate energy such as strain, melting, and fragmentation will be present to a greater or lesser extent depending on the speed and mass of the projectile. For this study, we were suspecting that phase changes in the material would dissipate some of the initial KE. To distinguish the amount of dissipation occurring, a point midway between both surfaces and 5 cm from the center of impact was monitored for maximum shear stress. This was done for each of the six cases and plotted in Figure 12. The phase changes induced by the lightest and fastest projectile succeeded in dissipating much of this KE. It can be seen from Figure 12 that projectile 1 produced a shear stress at a point 5 cm from the center of impact that is considerably below the maximum amplitude of the shear stress induced by the impact of the other 5 projectiles. The maximum amplitude of the shear stress for the other 5 projectiles were approximately the same. This is expected since their initial KE was constant and phase changes were not observed.

CONCLUSION

The series of calculations outlined in this paper have demonstrated the occurrence of energy dissipation in the early-time phase and the subsequent decrease in shear stress at latter-times. We have seen that phase changes occurring at the site of impact dissipate KE to such an extent that maximum shear stress is decreased by about 16 percent over slower projectiles with equal amount of KE. Since future breakup modeling will necessarily incorporate the effects of the early-time phase in order to predict the effects of the late-time phase, it is necessary to understand this dissipation phenomena.

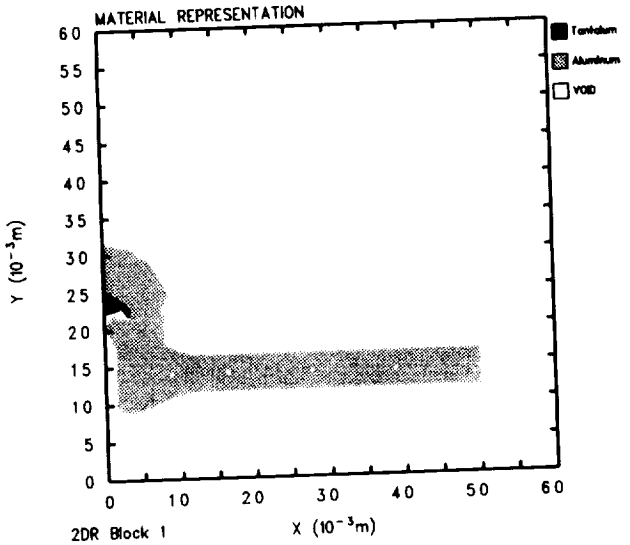

Figure 2. Model configuration of Case 1 at t = 1.27 μs.

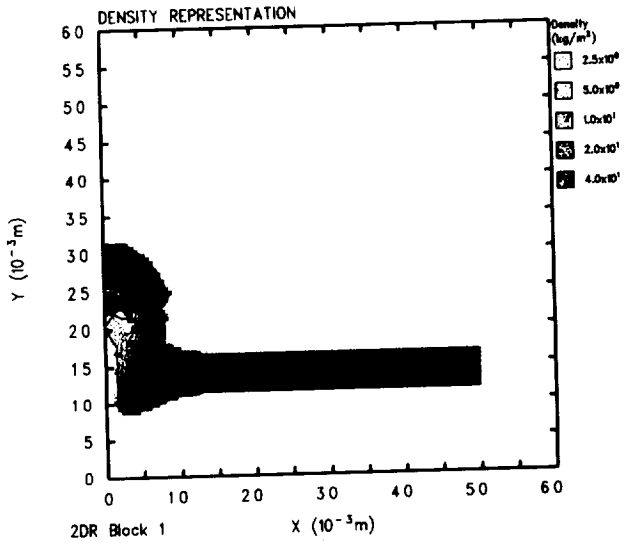

Figure 3. Density representation of Case 1 at t = 1.27 μs.

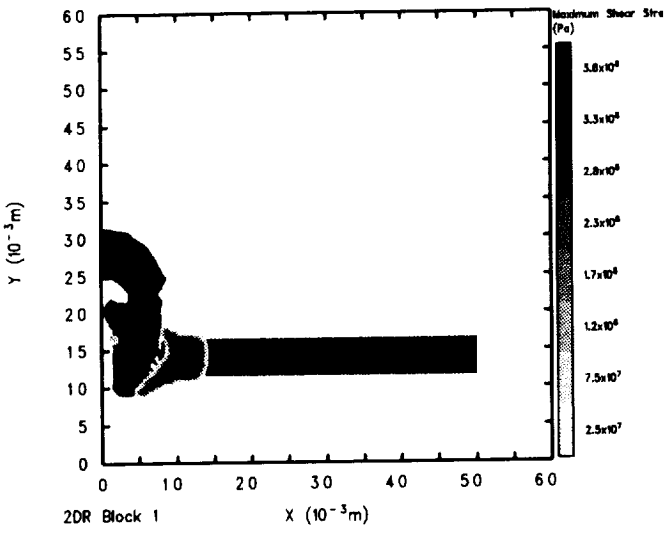

Figure 4. Maximum shear stress contour representation of Case 1 at t=1.27 μs.

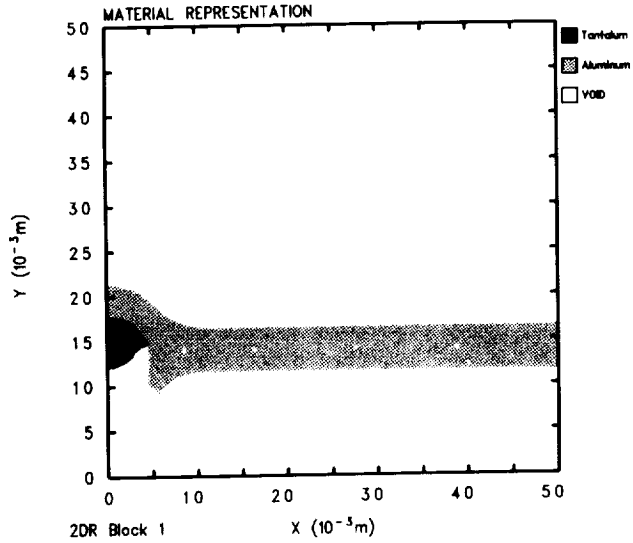

Figure 6. Model configuration of Case 2 at t=1.26 μs.

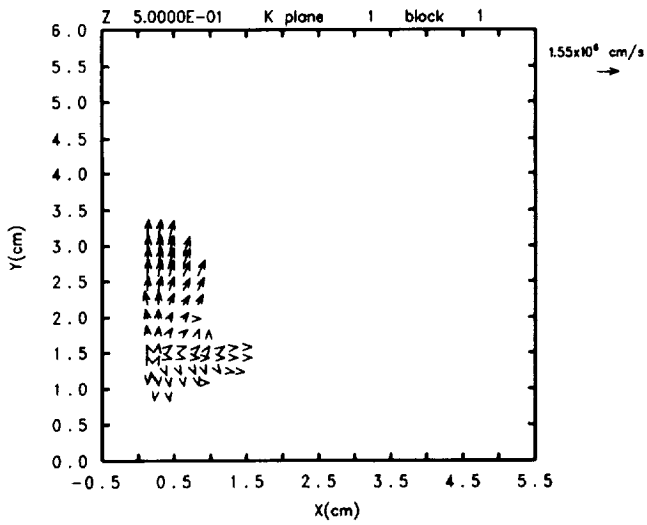

Figure 5. Velocity vector representaion of Case 1 at t=1.27 μs.

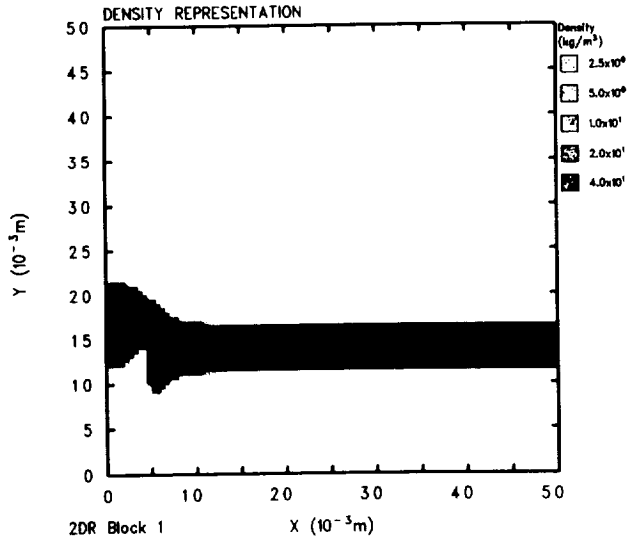

Figure 7. Density representation of Case 2 at t=1.26 μs.

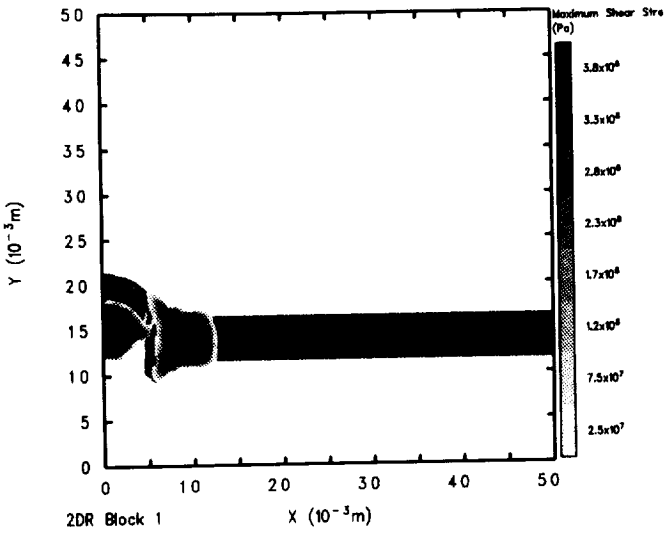

Figure 8. Maximum shear stress contour representation of Case 2 at t = 1.26 μs.

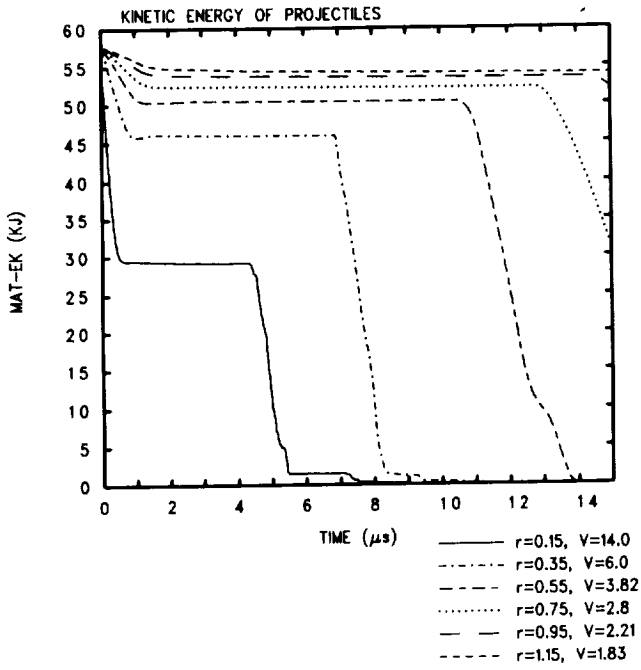

Figure 10. Total kinetic energy of the projectiles for the six cases.

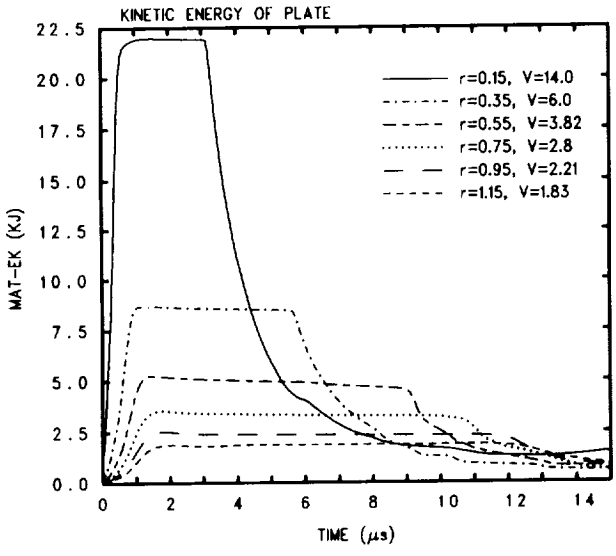

Figure 9. Total kinetic energy of the plate for the six cases.

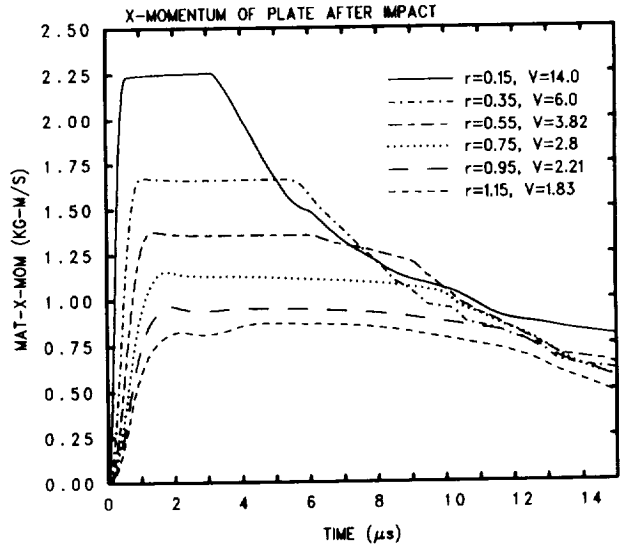

Figure 11. Momentum of plate after impact for the six cases.

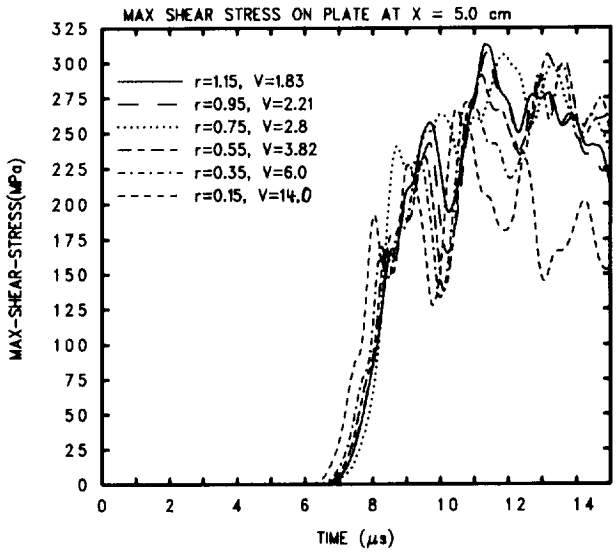

Figure 12. Maximum shear stress at 5 cm from center of impact for the six cases.

REFERENCES

1. McGlaun, J. M., et. al., **CTH User's Manual and Input Instructions**, Sandia National Laboratories, Version 1.020, July 90.

2. Wu, K. S. and G. A., Simon, "Optimization of Target Mass Distribution Against Impulsive Loading," Physical Sciences Inc., Report PSI-2039/TR-750, January 88.

3. Thompson, S. L., and Lauson, H. S., **Improvements in the Chart D Radiation-Hydrodynamic Code III: Revised Analytic Equations of State**, Sandia National Laboratories, Report SC-RR-71 0714, June 1985, pp. 62-65.